Measurements of the Nucleon Spin Structure at SLAC in End Station A

E143 COLLABORATION*

R. Arnold, P. Bosted, J. Dunne, S. Rock, Z. Szalata, J. White
American University, Washington D. C. 20016

D. Fritschi, J. Jourdan, G. Masson, S. Robinson, I. Sick
Institut für Physik der Universität, CH 4056 Basel, Switzerland

J. Gomez, J. Mougey, S. Nanda
CEBAF, Newport News, VA 23606

A. Thompson
Harvard University, Cambridge, MA 02138

P. Anthony, F. Dietrich, M. Mugge, K. van Bibber
Lawrence Livermore National Laboratory, Livermore, CA 94550

J. Button-Shafer
University of Massachusetts, Amherst, MA 01003

T. Chupp
University of Michigan, Ann Arbor, MI 48109-1120

K. Hicks
Ohio University, Athens, OH 45701

* Co-spokesmen: J. McCarthy, C. Prescott

V. Breton, H. Fonvieille,
LPC, Université Blaise Pascal, F63177 Aubière cedex FRANCE

D. Benton, K. Griffioen
University of Pennsylvania, Philadelphia, PA 19104

A. Bodek, P. de Barbaro, W. Sakumoto, R. Walker
University of Rochester, Rochester, NY14627

H. Borel, R. Lombard, J. Marroncle, J. Morgenstern, F. Staley, Y. Terrien
Saclay, F-91191 Gif sur Yvette cedex FRANCE

W. Atwood, J. Clendennin, T. Fieguth, R. Gearhart, E. Hughes,
T. Maruyama, W. Meyer, K. Moffeit, A. Odian, G. Petratos,
C. Prescott, L. Rochester, S. St. Lorant, T. Usher, M. Woods, C. Young
Stanford Linear Accelerator Center, Stanford University, Stanford, CA 94309

D. Kawall, S. Kuhn, Z. Meziani
Stanford University, Stanford, CA 94305

J.Lichtenstadt
Tel Aviv University, Tel Aviv, Israel

H. Baghaei, J. Chen, D. Crabb, D. Day, K. Keeter,
R. Lindgren, R. Lourie, R. Marshall, J. McCarthy, R. Minehart,
J. Mitchell, B. Norum, D. Pocanic, O. Rondon-Aramayo, C. Smith, S. VanVerst
University of Virginia, Charlottesville, VA 22901

H. Band, J. Johnson, R. Prepost, G. Zapalac
University of Wisconsin, Madison, WI 53706

ABSTRACT

The E143 Collaboration proposes measurements of the proton and neutron spin structure in SLAC's End Station A facility. With a beam energy of 22.66 GeV, the measurements will cover the range $0.03 \leq x \leq 1$ at momentum transfers greater than 1 $(\mathrm{GeV/c})^2$. Polarized ammonia and deuterated ammonia targets will be used in these measurements. The neutron spin structure is extracted from the polarized deuterium in the ND_3 target. The anticipated results will contribute significant new data and will serve to measure the Ellis-Jaffe sum rules to the 8% level for the proton and 19% level for the neutron, and the Bjorken sum rule to the 16% level, with statistical and systematic errors combined. The measurements rely mostly on existing End Station facilities that will be used by the preceding experiment E142. The contribution of the present experiment will be the use of new advances in polarized target and polarized beam technologies which will make possible a substantial reduction in systematic uncertainties.

Three months of calendar time are requested for check out and data taking.

1. Introduction

The successful acceleration of high energy polarized electrons at the Stanford Linear Accelerator Center opens up the possibility of using these beams for further electron-nucleon scattering experiments with fixed polarized or unpolarized nuclear targets. Among the important physics issues that can be addressed with them are the dependence of the spin structure functions of the nucleons on the Bjorken scaling variable x_B ($\equiv x$) and on the momentum transfer $-q_\mu^2 = Q^2$, and their integrals over the scaling variable. Past measurements of one of these quantities, the $g_1(x)$ (or longitudinal) spin structure of the proton, have revealed a substantial disagreement with the theoretical expectation of the Ellis-Jaffe sum rule leading to the current proton spin "crisis". This discrepancy will not likely be resolved until both the proton and neutron $g_1(x)$ and $g_2(x)$ functions are determined to adequate precision.

In the present case such determinations will make use of the following elements:

i) High energy polarized electron beams transported into the ESA;

ii) A set of ammonia based polarized proton and deuteron targets;

iii) The spectrometers and detector packages for particle identification;

iv) A beam polarimeter;

v) The data acquisition system based on the ESA Counting House electronics and computers.

Much of this equipment will be the same that experiment E142[1] will use for the measurement of the neutron spin asymmetry with a ^{3}He target, with suitable modifications to make it compatible with the solid state target design and operating conditions. The experience of E142 in operating and understanding the equipment will be of great value for the experiment being proposed here.

In what follows we will discuss the motivation for carrying out such a program at SLAC, and provide a summary of the experimental conditions, expected results and beam time requirements. The target, the spectrometers and the polarized electron source are described in greater detail in the corresponding sections.

2. Background, motivation, and experimental program

The spin structure functions appear as factors in the antisymmetric component of the hadronic tensor in the expression for the cross section for inclusive polarized lepton-polarized nucleon inelastic scattering. In the laboratory frame one has

$$\frac{d^2\sigma}{d\Omega dE'} = \frac{1}{2M}\frac{\alpha^2}{Q^4}\frac{E'}{E}(L^S_{\mu\nu}W^{S\mu\nu} - L^A_{\mu\nu}W^{A\mu\nu}). \qquad (1)$$

Here E and E' are the initial and final lepton energies, Ω is the lepton detector solid angle and M is the nucleon mass. The symbols S and A stand for the symmetric and antisymmetric parts, respectively. The sign of the antisymmetric part of the

hadronic tensor depends on the helicity of the nucleon in the lepton-hadron c.m. frame. Therefore, when we compute the sum and the difference of the cross sections for two orientations θ_N and $\theta_N + \pi$ of the nucleon spin, we have a cancellation of either the symmetric or the antisymmetric parts, respectively.

The sum is just twice the unpolarized cross section. On the other hand, the difference[2,3] is sensitive to the nucleon polarization. For $\theta_N = 0$ (i.e. longitudinally polarized leptons and nucleons) we get

$$\frac{d^2\sigma(0)}{d\Omega dE'} - \frac{d^2\sigma(\pi)}{d\Omega dE'} = \sigma^{\uparrow\uparrow} - \sigma^{\uparrow\downarrow} = \frac{4\alpha^2 E'}{Q^2 E}\Big((E + E'\cos\theta)MG_1 - Q^2 G_2\Big) \quad (2)$$

and for $\theta_N = \pi/2$ (longitudinal leptons and transverse nucleons) the result is

$$\frac{d^2\sigma(\pi/2)}{d\Omega dE'} - \frac{d^2\sigma(3\pi/2)}{d\Omega dE'} = \sigma^{\uparrow\rightarrow} - \sigma^{\uparrow\leftarrow} = \frac{4\alpha^2 E'}{Q^2 E} E' \sin\theta (MG_1 + 2EG_2) \quad (3)$$

where $G_1(Q^2, \nu)$ and $G_2(Q^2, \nu)$ are the spin structure functions. The latter can be related in the asymptotic limit to helicity distributions of the partons in the nucleon:

$$\lim_{Q^2,\nu\to\infty} (M\nu) MG_1(Q^2,\nu) = g_1(x), \qquad \lim_{Q^2,\nu\to\infty} (M\nu)\nu G_2(Q^2,\nu) = g_2(x). \quad (4)$$

The longitudinal cross section difference can be rewritten in terms of the unpolarized cross section $\sigma = d^2\sigma_{ep}/(d\Omega dE')$ and the longitudinal asymmetry $A = (\sigma^{\uparrow\uparrow} - \sigma^{\uparrow\downarrow})/(2\sigma)$ to obtain, as was suggested by Leader and Anselmino,[4] the following expression[5] for the asymptotic structure functions:

$$g_1(x) - k g_2(x) = 2K\sigma A. \quad (5)$$

where k and K are kinematical factors defined in the Appendix. A similar equation can be written for the transverse combination:

$$g_1(x) + k' g_2(x) = 2K'\sigma A'. \quad (6)$$

Here A' refers to the transverse asymmetry $A' = (\sigma^{\uparrow\rightarrow} - \sigma^{\uparrow\leftarrow})/(2\sigma)$, and k', K' are found in the Appendix.

Equation (5) can be compared with the conventional approximation for g_1 (in which the contribution of g_2 has been neglected):

$$g_1(x) \simeq \frac{F_2(x)}{2x(1+R(x))} A_1(x). \tag{7}$$

The extraction of g_1 from this expression, in contrast to (5), requires knowledge of the unpolarized structure function F_2 and the ratio R of the longitudinal to transverse photon absorption cross sections. The spin asymmetry A_1, which describes the relative difference between the helicity flip and non-flip virtual photon absorption cross sections is obtained from the approximate relation $A_1 \simeq A/D$ (D is the virtual photon depolarization factor, a function of R and the scaling variable $y = (E - E')/E$, defined in the appendix).

Measurements of the spin asymmetry A_1^p of the proton have been carried out in the past at SLAC[6,7] and at CERN.[8] While a variety of models of A_1 for the proton seem to agree with all the experimental results in the range of the scaling variable $0.1 \leq x \leq 0.7$, the experimental uncertainties are large and the comparison with the theoretical predictions is inconclusive. On the other hand, in the range $0.01 \leq x \leq 0.1$, the EMC results lie below the predictions of all the models. Moreover, it has been found that the integral $\int_0^1 g_1^p(x)dx = 0.126 \pm 0.01 \pm 0.015$ of the combined experimental data falls short of the prediction $\int g_1^p(x)dx = 0.198 \pm 0.005$ for this sum rule formulated by Ellis and Jaffe[9] by more than four standard deviations.

A very extensive literature on this discrepancy has been generated in the past four years, dwelling mainly on the different theoretical interpretations of the EMC result. While questions such as the effects of the variation in momentum transfer for the data points measured by the past experiments, or the applicability of the parton model to the interpretation of the data, need to be resolved, it remains true that the definitive solution of the problem will require a precise and accurate remeasurement of the structure function g_1^p , and measurement of the complementary neutron function g_1^n in the broadest ranges of x and Q^2. Special emphasis on the small x region, for which only the EMC data are presently available, will be critical. In

fact, were it not for the five EMC data points in the region $x < 0.1$, the combined SLAC-CERN data would still be compatible with the Ellis-Jaffe prediction. The importance of determining the true value of the proton integral and of the combined proton-minus-neutron integrals, also known as the Bjorken sum rule[10]

$$\int (g_1^p - g_1^n) dx = \frac{1}{6} \left| \frac{g_A}{g_V} \right|_{n \to p e^- \bar{\nu}} \left(1 - \frac{\alpha_s(Q^2)}{\pi} \right) \tag{8}$$

(with QCD corrections for finite Q^2) has been often asserted in the literature, making any new review unnecessarily repetitive.

The second structure function g_2 is a quantity worthy of study in itself. g_2 has been mentioned in the literature since the sixties.[10] Theoretical studies of g_2 have yielded an exact sum rule,[11] $\int_0^1 g_2\,(x) dx = 0$ and an approximate one.[12] Feynman[13] interpreted g_2 in the parton model as contributing, with g_1, to the transverse quark spin density of a transversely polarized proton. The meaning of g_2 in this model has been clarified by Leader and Anselmino,[4] who obtain $g_2 \neq 0$ if transverse components of the parton motion are present, and find that g_2 diverges as $1/x$, thus invalidating the first sum rule. In fact, a Regge pole analysis[14] predicts an even stronger divergence for g_2 : $x^{-1-\alpha_c}$ with $\alpha_c = 1$. In more recent studies new sum rules have been obtained.[15] Jaffe and Ji[16] concluded in their operator-product expansion analysis of g_2 that twist-3 contributions, reflecting quark-gluon interactions, are significant in g_2 , and that its measurement would be a unique opportunity to study them. The extraction of g_2 from the measurement of transverse asymmetries in polarized electron-nucleon scattering[2,3] is an especially favorable technique, as pointed out by our own estimates discussed later in the proposal, as well as by the analysis of Hidaka *et al.*[17] These authors established, in addition, that the transverse spin asymmetry in proton-antiproton scattering would be exceedingly hard to measure, although it has been pointed out that Drell-Yan muon pair production may be a feasible alternative in $p - \bar{p}$ scattering.[18]

The present proposal is part of a complete program of studies which initially does not require major modifications of the beam transport optics and would cover

the range of x attainable with the highest energy beams that can be transported at the present time into the End Station A. At a future time, an extension of the measurements to smaller x values, and Q^2 dependence studies, will be proposed. This would take place at the first opportunity after the modifications required to transport 50 GeV beams into the ESA are completed.

To carry out the proposed measurements, the target will first be polarized parallel to the longitudinally polarized beam to determine (for both the proton and the deuteron) the corresponding combination of the structure functions g_1 and g_2 in Eq. (5) . Measuring both the proton and the deuteron spin structure, under identical experimental conditions, with systematic effects affecting both targets in the same way, is the closest that an experiment can get at extracting the free nucleon polarized structure functions and testing the Bjorken sum rule. Furthermore, the data to be obtained in this experiment will complement the measurements on ^{3}He expected from experiment E142. Both data sets will have basically identical kinematics, and their combination will bring us even closer to the ideal of understanding the properties of the free nucleon.

The combination of g_1 and g_2 in Eq. (6) that depends on transverse target polarization will be measured with the corresponding transverse-to-the-beam target orientation. This measurement, combined with that of the longitudinal asymmetry, will be used to extract both structure functions. The transverse polarization capability of the target is especially valuable in view of the lower energies available at SLAC relative to the muon beam laboratories: Neglecting the contribution of g_2 to the longitudinal asymmetry, (or conversely, the contribution of the transverse asymmetry to g_1^p) as it was done in the analysis of the EMC data, would lead to larger systematic errors at lower energy. In summary, the determination of g_2 will not only improve our knowledge of g_1 but it will also directly probe the parton model in the more realistic regime of finite transverse motion, with off-shell partons, and it will test the validity of the operator-product expansion and Regge pole results.

3. Experimental method

The experiments will involve several steps:

- Determination of the $g_1^p - kg_2^p$ combination from the expression

$$g_1^p - kg_2^p = 2K\sigma A. \tag{9}$$

The unpolarized cross section σ will be measured in the experiment, together with the longitudinal asymmetry A which will be determined from the measured asymmetry Δ. The latter is defined in terms of the number of events N with a given orientation of the beam and target polarizations (parallel or opposite):

$$\Delta = \frac{N^{\uparrow\uparrow} - N^{\uparrow\downarrow}}{N^{\uparrow\uparrow} + N^{\uparrow\downarrow}} = P_b P_t f(1+C)A, \tag{10}$$

which depends on the polarizations of the beam $P_b(\sim 0.8)$ and the free protons in the target $P_t(\sim 0.9)$, and on the dilution factor $f(\sim 0.12)$, which represents the ratio of the probability of scattering from a free proton to the probability of scattering from all the nucleons in the target. The correction term C includes the effects of the nitrogen polarization in the ammonia molecule, and is of the order of 1.5%.

In this step, g_2^p can be treated as an unknown, contributing a substantial systematic uncertainty in the extraction of g_1^p .

- Determination of the $g_1^d - kg_2^d$ combination for the deuteron, in a similar fashion as above. Of course, the values of P_t, f and C in this case correspond to the deuteron target.

- Extraction of the combination $g_1^n - kg_2^n$ for the neutron from the deuteron and proton asymmetries. The neutron asymmetry is given by

$$A_n = (1 + \frac{\sigma_p}{\sigma_n})\frac{A_d}{\gamma} - (\frac{\sigma_p}{\sigma_n})A_p \tag{11}$$

where σ_p/σ_n is extracted from deep inelastic scattering data. $\gamma \simeq 0.92$ is the

effective polarization of the nucleons in the deuteron, correcting for those in the D-state.

• Determination of the $g_1^p + k' g_2^p$ combination from the expression

$$g_1^p + k' g_2^p = 2K' \sigma A', \tag{12}$$

where A' is the transverse cross section asymmetry, and k' and K' are the corresponding kinematic factors. The polarized target field will be aligned transverse to the beam direction in this case.

• Determination of the $g_1^d + k' g_2^d$ combination. This measurement may receive higher priority than the A' for the proton, since the g_2 component here represents a greater uncertainty for the extraction of g_1^d than it does for g_1^p .

• Spectrometer studies. These studies are required in view of the method proposed which involves the determination of the absolute unpolarized cross section σ to a precision better than that obtainable using the measured unpolarized structure functions F_2 and R (extrapolated to the kinematic region of our proposal) from other experiments. They involve applying various techniques such as e–p elastic scattering, momentum sweeps, using metal targets, etc.

As stated earlier, this proposal covers the range $0.03 \leq x \leq 1$, for values of the momentum transfer Q^2 greater than 1 $[\mathrm{GeV/c}]^2$. This kinematic region will be explored by means of appropriate arrangements of spectrometers in the ESA, using electron beams of 22.66 GeV or higher energy, with longitudinal polarizations of 80%, that can be transported into the ESA and scattered on the polarized solid ammonia (NH_3 and ND_3) targets, 2.5 cm in length. Target polarizations greater than 90% for protons and 45% for deuterons are the conservative expectations at this time. At repetition rates of 120 pulses per second the heat deposition in the target limits the beam currents to about 2×10^9 electrons per linac pulse. For the run times proposed the resulting count rates will allow the accumulation of the required numbers of counts, in order to obtain statistical uncertainties smaller

than the systematic ones. In addition a beam rastering system to reduce the instantaneous heat load in the target will be needed.

The capabilities of the target, which has a wide range of polarization orientations, will be exploited. This target is based on irradiated ordinary (NH_3) and deuterated (ND_3) ammonia beads, solidified at $1K$ or lower temperatures and operating in a magnetic field of 5T. Under these conditions, ammonia has been shown[19,20] to have superior radiation resistance, allowing for high polarizations, luminosities of the order of $40 \times 10^{33} cm^{-2} s^{-1}$ and quick recovery of polarization losses. An open geometry superconducting Helmholtz coil provides the magnetic field to align the nuclei by the method of dynamic nuclear polarization.

The details of the spectrometer arrangements and associated detector packages will closely follow their counterparts of the set up for experiment E142, which plans to measure g_1^n under similar kinematic conditions and beam parameters. Two similar non-focussing spectrometers, placed at 4.5° and 7° will be used to cover the low and high regions of x. The small angle spectrometer will cover the range $0.03 \leq x \leq 0.316$ for Q^2 values from ~ 1 (GeV/c)^2 at low x to 2.5 (GeV/c)^2 at the upper end. The 7° spectrometer will cover the range $x = 0.1$ to $x = 1$. The corresponding Q^2 values are 2.9 and 6.4 (GeV/c)^2 at the low and high x respectively. The region of overlap between both spectrometers ($0.1 \leq x \leq 0.316$) will provide information on the Q^2 dependence of the structure functions. For this region, the average Q^2 at 4.5° is 2.3 (GeV/c)^2 while at 7° it is 4.6 (GeV/c)^2.

Electrons will be identified and their momentum measured by a combination of hodoscopes, Čerenkov detectors and shower counters, which will also provide adequate background rejection. The ESA counting house electronics and computers will be used for the data acquisition. Finally, a beam polarimeter of the coincidence Møller type is planned.

4. Expected Results and Run Plan

The x dependence of the structure function g_1^p will be measured with the point statistical uncertainties shown in Fig. 1. They lie in the range of 4 to 12%, with the exception of endpoints where the maximum uncertainty will be 20%. Only statistical errors for the EMC data are displayed.

In the case of deuterium, shown in Fig. 2, the statistical uncertainties correspond to a minimum sensitivity in g_1^d of 0.03 near the predicted zero crossing on the small x side and 0.05 on the large x side.

The systematic uncertainties can be divided into two groups: those that come from factors that have an x dependence (such as the dilution factor f); and those that represent an overall normalization uncertainty, such as the beam polarization P_b (although they may have a time dependence). For the x dependent factors, the uncertainties will be on the order of 3% or less, while the normalization uncertainty is expected to be less than 6%. A detailed discussion of these errors is given below.

Letting $N^{\uparrow\uparrow} + N^{\uparrow\downarrow}$ represent the net number of detected electrons (corrected for detector efficiency, dead time losses and pion and e^+e^- pair contamination) the following expression for the unpolarized cross section σ can be used:

$$\sigma = \frac{N^{\uparrow\uparrow} + N^{\uparrow\downarrow}}{2\mathcal{A}\mathcal{Q}d} R_c, \tag{13}$$

where the symbol $\mathcal{A}$ represents the spectrometer acceptance, $\mathcal{Q}$ is the total number of beam particles incident on target for both orientations of the beam and target polarizations (i.e. the beam "charge"), d is the total target thickness in cm^{-2} and R_c stands for the radiative correction factor. We can then rewrite using Eq. (10)

$$g_1(x) - kg_2(x) = 2K\sigma A = K\frac{(N^{\uparrow\uparrow} + N^{\uparrow\downarrow})R_c}{\mathcal{A}\mathcal{Q}d} \cdot \frac{\Delta}{fP_bP_t(1+C)}, \tag{14}$$

where $k, K, \mathcal{A}, R_c, f$, and C are x dependent terms.

The contributions of the factors in (14) to the uncertainty in the combined quantity $g_1 - kg_2$ are as follows:

Table 1. Sources of systematic errors

Source	Factors	Maximum contribution
(x dependent)		
Acceptance	$\mathcal{A}$	3%
Kinematic factor K	E, E', θ	3%
Dilution factor	f	3%
Nitrogen correction	C	0.5%
Radiative correction	R_c	< 3%
$\pi, e^+ - e^-$ contamination		<1%
(x independent)		
Beam polarization	P_b	3%
Target polarization	P_{NH_3}, P_{ND_3}	3%, 6%
Target thickness	d	3%
Charge	$\mathcal{Q}$	1%
Dead time, efficiency		<1%

In addition, in the case of the deuteron, the small D-state probability correction contributes an uncertainty estimated from the variance of the different models for the nuclear wave function to be 1.8% of γ.

The measurement of the combinations $g_1 + k'g_2$, or equivalently, the measurement of the transverse asymmetry A', yields a double benefit: g_2 can be determined to the same relative precision as A', and the contribution of A' (through the kg_2 term) to the longitudinal structure function g_1 can be reduced. Estimates of the upper limit of g_2 are based on the positivity condition $|A_2| \leq \sqrt{R}$ obeyed by the spin asymmetry A_2, where R is the ratio of longitudinal to transverse cross sections defined earlier. Based on these estimates, it can be shown that the transverse

asymmetries A' could be of the order of 20 to 30%, and therefore about two to more than four times as large as the longitudinal asymmetries A in the region $0.03 \leq x \leq 0.2$ where g_2 is greatest. Hence, a measurement of g_2 with reasonable precision could be done in a fraction of the time requested for the g_1 run. The expected results of such measurement of g_2^p are shown in Fig. 3, which displays the sensitivity of the measurement of A' for data taking time equal to one fourth the length of that proposed for the measurement of the longitudinal asymmetry, as given in the run plan Table 4 below.

The transverse measurements have the same systematic and normalization uncertainties as the longitudinal ones, with the difference that K' is the appropriate kinematic factor, contributing again a maximum of 3% systematic uncertainty.

The propagation of the systematic errors to the integrals of the spin structure functions over the measured x region is displayed in Tables 2 and 3 below:

Table 2. Expected errors

Integral	Statistics	Systematic x-dependent	Systematic x-independent	$\delta A'$	D-state
$0.03 \leq x \leq 1$		$\delta(f,K,C,\mathcal{A},R_\epsilon)$	$\delta(P_b,P_t,d,\mathcal{Q})$		
$\int g_1^p = 0.126$	0.002	0.008	0.007	0.002	–
$\int g_1^d = 0.057$	0.003	0.004	0.003	0.004	0.001

The $\delta A'$ contribution shown here is the integral of the uncertainty in the proposed measurement of A'.

Table 3 summarizes the expected results. The values for the integrals have been estimated using the combined EMC and SLAC-Yale result for the proton sum, and the Bjorken sum rule. Combined quadratic sums of the systematic x-dependent and normalization errors are shown. The magnitude of the relative uncertainties is independent of the actual results for the integrals.

Table 3. Expected results

Integral $0.03 \leq x \leq 1$	Sum	Statistical error	Systematic error
$\int g_1^p dx$	0.126	$\pm$0.002 (2%)	$\pm$0.010 (8%)
$\int g_1^d dx$	0.057	$\pm$0.003 (6%)	$\pm$0.006 (11%)
$\int g_1^n dx = \frac{1}{\gamma}\int g_1^d dx - \int g_1^p dx$	-0.066	$\pm$0.004 (6%)	$\pm$0.013 (19%)
$\int (g_1^p - g_1^n) dx = 2\int g_1^p dx - \frac{1}{\gamma}\int g_1^d dx$	0.191	$\pm$0.005 (3%)	$\pm$0.022 (12%)

The last entry in the table represents the Bjorken sum rule (BSR). Since this rule is only valid for the full range $0 \leq x \leq 1$, one needs to estimate the contribution of the unmeasured x region. To estimate this we have extrapolated down to $x = 0$ using the modified Callaway-Ellis model[5] that fits both the combined EMC-SLAC-Yale integral of g_1^p and the QCD corrected BSR. The area under the extrapolated region is 0.011 for g_1^p and -0.01 for g_1^d. Taking, à *la* EMC, the values of these areas to be equal to their uncertainties, the resulting systematic error in the BSR is 0.03, or 16%. Better determinations of the extrapolation will be made by combining the actual results of the present experiment with those of related past and current experiments.

The counting rates in all cases will be ≤ 1 electron per beam pulse, per spectrometer, limited by beam heating of the target, implying that the

following data taking times will be required:

$g_1^p - k g_2^p$	100	hours
$g_1^d - k g_2^d$	160	hours
$g_1^p + k' g_2^p$	25	hours
$g_1^d + k' g_2^d$	40	hours
Spectrometer studies	260	hours

For polarized beam and target running an overhead time is expected to be equal to the data taking time. The overhead will be for for target annealing about every 4 hours, target polarization reversals (done by re-tuning the microwave frequency) , and Møller polarimetry. In addition we request two weeks of checkout beam before the main data runs to commission the polarized target and a new coincidence Møller polarimeter, and to reestablish the operation of the spectrometers, detectors, data acquisition system, beam steering, and other equipment. Considering a laboratory efficiency of 50%, a total of 2160 hours are requested, or three calendar months including check out.

These times will be distributed as shown in the run plan detailed in Tables 4a, b, and c.

Table 4a. Run Plan - Spectrometer studies

Item	Energy, Angles	Operations	Time (total)
Acceptance	22.66 GeV; 4.5°, 7°	Data runs	260 hours

Table 4b. Run Plan - Longitudinal Polarizations: $\beta_e \parallel B$ †

Item	Target	Energy, Angles	Operations	No.	Time (total)
$g_1^p - kg_2^p$	NH_3	22.66 GeV; 4.5°, 7°	Data runs	25	100 hours
			Overhead		100 hours
			Subtotal		200 hours
$g_1^d - kg_2^d$	ND_3	22.66 GeV; 4.5°, 7°	Data runs	40	160 hours
			Overhead		160 hours
			Subtotal		320 hours

Table 4c. Run Plan - Transverse Polarizations: $\beta_e \perp B$

Item	Target	Energy, Angles	Operations	No.	Time (total)
$g_1^p + k'g_2^p$	NH_3	22.66 GeV; 4.5°, 7°	Data runs	6	25 hours
			Overhead		25 hours
			Subtotal		50 hours
$g_1^d + k'g_2^d$	ND_3	22.66 GeV; 4.5°, 7°	Data runs	10	40 hours
			Overhead		40 hours
			Subtotal		80 hours
Total (5 items)					910 hours
Laboratory efficiency (50%)					910 hours
Checkout (two weeks)					340 hours
			Grand Total (three months)		2160 hours

† β_e represents the electron velocity (helicity:$\pm 1/2$); **B** is the target magnetic field.

5. Solid Polarized Proton and Neutron Targets

Solid polarized targets work on the principle of Dynamic Nuclear Polarization in which a target material such as butanol, ethylene glycol, or ammonia, is doped, by chemical or radiation techniques, with a dilute assembly of paramagnetic atoms. The material is cooled to ≤ 1K in a magnetic field of a few Tesla and then irradiated by microwaves to drive the hyperfine transition which allows the nucleon (nuclear) spins to be aligned. All elements present in the material which possess a magnetic moment can be polarized at the same time. For spin-1/2 the polarization P is given by:

$$P = \tanh[\mu B/kT]$$

where μ is the magnetic moment, B is the magnetic field, k is Boltzman's constant and T is the spin temperature.

For many particle scattering experiments the choice of a polarized target is dictated by the requirement that a basic figure of merit, F, of the type

$$F = P^2 I$$

be as large as possible. Here P is the polarization and I is the beam intensity. For example in the case where I is limited for some reason the choice would likely lead to a dilution refrigerator. Operation at very low temperatures would mean proton polarizations of greater than 90%.

However for E143 the beam intensities are such that the material must be very resistant to radiation damage and must operate in a cryogenic environment which allows the most efficient removal of heat deposited by the beam. For these reasons the target system will be a ^{4}He evaporation refrigerator operating with a magnetic field of 5T. The target material will be radiation doped ammonia[21] (NH_3 and ND_3). The equipment has been designed and will be assembled at Virginia.

^{4}He is used because of its superior thermal properties compared to ^{3}He. Only 1K can be reached with ^{4}He so a 5T magnet is necessary to at least maintain the polarization which can be achieved by using ^{3}He at 0.5K in a field of 2.5T.

Ammonia is the material of choice because of its resistance to radiation damage and its higher hydrogen or deuterium content compared to other materials.

Past experience at SLAC with a 5T/1K target[22] showed that operation with materials such as butanol doped with porphyrexide was limited by the radiation damage inflicted on the material. A large overhead in time was incurred because of the necessity to change the target at frequent intervals. Subsequently it was found, at Bonn,[23] at SLAC[19] and Michigan[24] under varying cryogenic conditions, that substantial polarizations could be obtained with radiation doped ammonia and that the radiation resistance was much better.

Development continued at Bonn, particularly with ND_3,[25] and at Michigan where it was found[20] that NH_3 could be quickly polarized to >90% in a 5T/1K system. This is shown in Fig. 4. At the AGS this target was used in a scattering experiment[26] using proton beams with intensities of up to 10^{11} protons/sec. Results from this experiment of relevance to E143 are:

1) Radiation damage: the e^{-1} value for the initial fall of polarization with beam dose is 4×10^{15} protons/cm^2, a factor of ten better than the best chemically doped material. This is in very good agreement with the data of Seely et al.[27] from an electron beam at SLAC. After about 10^{15} protons pass through the target the radiation damage rate slows down giving an e^{-1} value of 1.3×10^{16} protons/cm^2. This is also in good agreement with the electron data.[27] In addition ammonia can be repeatedly annealed without loss of polarization, in contrast to chemically doped materials which have to be replaced after a few anneals.

2) Beam heating: with the ^{4}He cryostat used at the AGS a beam of 8×10^{10} protons/sec could be directed onto the target with a loss of only 2% in polarization. For a ^{3}He system a beam of 2×10^{10} protons/sec reduced the polarization by 15%.

3) Annealing: generally the target was annealed when the polarization fell to about 80%. On the basis of the radiation damage values given in 1) a total of 3.25×10^{15} protons passes through the target while the polarization falls from 97% to 80%. For E143 running at 2.5×10^{11} electrons/sec this would mean annealing every 3.5 to 4 hours.

4)Polarization: the polarization is relatively insensitive to the bulk temperature. Even at 1.6K values of >70% were reached in 20 minutes.

Overall, an improvement of a factor of 12 in the figure of merit F, was achieved at the AGS by using this 5T/1K ^{4}He target instead of the older 2.5T/0.5K ^{3}He target. There was also an increase in the operational efficiency. In comparison with the SLAC 5T/1K target used in previous experiments, with butanol as the target material, an increase in F of a factor of 10 should be obtained with our ammonia target. We can also expect an increase in operational efficiency.

The radiation damage properties of ND_3 have been studied extensively by the Bonn group. Deuteron polarizations of about 50% have been obtained at 3.5T/0.3K with corresponding proton polarizations of about 100%. The only measurement of ND_3 at 5T/1K, at SLAC, yielded polarizations of 25% but with proton polarizations of 75%. Under the same conditions as for NH_3 in the Michigan target a deuteron polarization of 45% is a reasonable assumption.

The disadvantage of using ammonia as a target in an experiment such as E143 is that the nitrogen is also polarized (up to about 20%). In the case of ^{14}N (spin 1) both the unpaired neutron and proton are polarized. But for ^{15}N (spin 1/2) there is only an unpaired proton to carry the polarization. The use of $^{15}ND_3$ and $^{15}NH_3$ as targets has several advantages the most important being a reduction in the systematic errors on the both the neutron and proton spin structure asymmetries.

Finally the status of the major target components is discussed:

a) 5T Magnet

The magnet has been ordered from Oxford Instruments and is due to be de-

livered to Virginia in Feb. 1992. A drawing of the magnet is shown in Fig. 5.

b) 1K ^{4}He Refrigerator

The refrigerator is designed to be integrated into the 5T magnet. It is very similar to the Michigan/Liverpool refrigerator discussed above. Provision has been made to install both proton and deuteron targets in the same cryostat and to be able to move either one into the beam easily. It has been ordered from Oxford Instruments and should be delivered with the magnet.

c) Microwave system

All components for the 140 GHz system have been assembled at Virginia. The microwave generator, an Extended Interaction Oscillator from Varian Canada, has been tested and provides a power of about 20W at 140 GHz.

d) NMR

Three of the standard Liverpool NMR detectors are on hand at Virginia. They have been tuned with a dummy coil. Other electronics for measurement and control are being developed.

e) Ammonia targets

An apparatus has been set up to freeze ammonia and break it into appropriate size fragments. Some $^{14}NH_3$ has been produced in the form of 2.5 mm granules. Irradiation methods are being discussed. All tests will be made with ^{14}N material before irradiating the ^{15}N material.

The complete polarized target is expected to be assembled and commissioned during summer 1992 and shipped to SLAC in Fall 1992.

6. Polarized Electron Source

A polarized electron source based on photoemission from negative-electron-affinity GaAs is the only source capable of meeting the high peak current requirements for injection into accelerators such as the SLC. This type of source was pioneered at SLAC and operated successfully in the SLAC parity violation experiment producing in excess of 10^{11} electrons in a 1.6 μsec pulse with an average polarization of 37%. Such a source is ideally suited to the needs of E143.

The maximum polarization obtainable from unstrained GaAs or from alloys such as AlGaAs is limited to 50% by the degeneracy of the two highest valence bands. These two bands allow transitions to opposite spin states in the conduction band. A strain in GaAs, on the other hand, lifts the degeneracy between the valence bands and in principle allows selective excitation of a single band transition to a single spin state in the conduction band, leading to 100% polarization if the strain is sufficiently large and close to ideal.

Such strained GaAs cathode structures are now under development at SLAC and independently at Nagoya University. The development of these cathodes has followed a recent breakthrough by a SLAC/University of Wisconsin collaboration which demonstrated electron spin polarization in excess of 70% using a strained epitaxial layer of InGaAs grown on a GaAs substrate.[28]

Current high polarization cathode developments utilize a strained epitaxial layer of GaAs grown on GaAsP. These structures are under study at both SLAC and Nagoya University.[29] Polarizations in excess of 85% have been achieved in both laboratories. A sample recently tested at SLAC yielded a polarization of 80% at 825 nm with a quantum efficiency of 10^{-3} and a lifetime of one week. This sample is already a practical cathode for E143. Studies are underway to improve the quantum efficiency by optimizing parameters such as the epitaxial layer thickness and the phosphorus concentration. Fig. 6 shows electron beam polarization as a function of excitation photon wavelength for such a strained GaAs photocathode tested at SLAC.

E143 requires a peak beam current of 0.2 mA in a 2 μsec pulse, corresponding to 0.5 mA at the source. Such a current can be achieved by a 825 nm 7.5 Watt laser with a cathode quantum efficiency of 10^{-4}. One possible solution is to chop the output of a CW Ti:Sapphire laser pumped by an Ar ion laser. Four such lasers, each operating at 5 Watts, are now running at SLAC for the optical pumping of the E142 He^3 target. These lasers should be available for E143.

A new polarized electron gun has been designed and built for the SLC and should be available for running E143 with the new cathode structures discussed above. This gun, based on the design of the SLC thermionic gun, is required to produce up to 2×10^{11} electrons in a 2 nsec pulse at 120 Hz (see Fig. 7). The gun was installed on the accelerator during the 1991 fall downtime.

The SLC polarized gun may be used for E143 without hardware modification. Because of the low peak beam current required for E143, the gun high voltage may be reduced to 70 kV without running in a space-charge limited mode. This reduced voltage level should eliminate the possibility of any high voltage breakdown in the gun.

In summary, the technology is now available for a high polarization cathode for E143. It should be possible to achieve 80% polarization at the modest E143 beam current requirements utilizing the newly developed strained GaAs cathodes and existing laboratory lasers. Research will continue during the coming year to optimize the parameters for maximum quantum efficiency, lifetime, and polarization.

7. Spectrometer Systems and Detectors

This section describes the two magnetic spectrometer systems to be used in this experiment. They were originally designed for experiment E142[1] which will measure the neutron g_1 spin-dependent structure function using a polarized ^{3}He target in the same kinematical domain as this experiment. The two spectrometers will be centered about 4.5° and 7.0°, which are the optimum scattering angles corresponding to the maximum polarized electron beam energy presently available (22.66 GeV). A momentum acceptance ranging from 7 to $\sim$ 19 GeV/c is required at those angles to cover the desired range in the Bjorken x from 0.03 to 1. A schematic layout of the two systems is shown in Fig. 8.

The design of the two systems was driven by several requirements. The cross sections to be measured are known to be small, typically of the order of 10^{-32} cm^2/sr/GeV. The asymmetry in the cross sections of the two different spin orientations is predicted to be also small, of the order of 10^{-3}. In order to minimize the beam running time, the spin structure function measurements require spectrometers with the largest possible solid angle over a momentum acceptance range extending from 7 to beyond 19 GeV/c.

In addition, these small scattering angle spectrometers should be able to suppress an expected large photon background coming from the target due to bremsstrahlung radiation, radiative Møller scattering and the decay of photoproduced π° mesons. Background rate estimates[30] have indicated the need for a 'two bounce system' (the shape of the spectrometer aperture should allow a photon to reach the detectors only after bouncing twice on the magnet or vacuum chamber walls) in order to keep this background at a tolerable level.

The momentum resolution of the spectrometers is defined solely by the required x resolution. A resolution in x ranging from ± 0.003 at x=0.03 to ± 0.09 at x=0.9 ($\Delta x/x = \pm 0.10$) is considered adequate for the needs of the asymmetry measurements. This translates to a required momentum resolution that varies from $\pm 6.9\%$ at E'=7 GeV/c to $\pm 2.0\%$ at $E' \simeq 19$ GeV/c for both spectrometers.

Past designs for polarized deep inelastic scattering experiments at SLAC[31] have achieved a solid angle peaking at a maximum value of 0.6 msr for the central momentum but falling rapidly on either side of the relative momentum. The designs were based on two large aperture dipole magnets both bending in the same direction. A new design[32] with the two dipoles bending in opposite directions provides a solid angle peaking at the same maximum but remaining constant over a very large momentum interval. For comparison, the solid angle of the 'reverse bend' dipole doublet configuration, when integrated over the 7 to 18 GeV momentum interval, is twice than that of the 'conventional' configuration. The solid angle of the two spectrometers is shown as a function of momentum in Figs. 9 and 10.

The reverse bend can also fulfill the 'two bounce' requirement by properly choosing the deflecting angles and the separation of the two dipoles. In this design, the bend plane position of the scattered particles at the detectors depends weakly on relative momentum. This results in a loss in momentum resolution (not critical in the experiment) but spreads out the pion background, which is highly peaked at 7 GeV, onto a large detector area, allowing measurements at a fairly large pion rate.

The purpose of the quadrupole in the 4.5° spectrometer is to increase the angular magnification in the non-bend plane and spread the scattered particles onto a larger detector area in this direction. In the bend-plane the quadrupole focusing improves the momentum resolution of the system and provides a solid angle roughly constant with momentum. The introduction of the quadrupole relaxes the instantaneous detector rate on the detector allowing accumulation of data in parallel and at the same rate with the 7° spectrometer.

Each spectrometer will be instrumented with a pair of Čerenkov detectors,[33] a pair of finely segmented scintillator hodoscopes[34] and a segmented lead-glass calorimeter of 24 radiation lengths in a fly's eye arrangement. The shower counter calorimeter will be assembled from a subset of the lead glass package[35] of the ASP experiment at the PEP ring. The electrons will be distinguished from the large pion

background using the pair of gas threshold Čerenkov counters in coincidence. The pair of hodoscopes will provide tracking information as well as timing information to assist in pion rejection.

The scattered electron energy will be measured by two methods. The first one will use the track information from the two hodoscopes and the known optical properties of the magnetic spectrometer. The second one will rely on the energy deposited in the lead-glass calorimeter. The scattering angle is measured with very good resolution by using the hodoscope track information. The fine segmentation of the shower counter can also provide a measurement of the scattering angle with resolution sufficient for the needs of the experiment.

The lead glass counter will be calibrated with a sample of scattered electrons of known energy in special elastic electron-proton runs using a gaseous hydrogen target at the beginning of experiment E142. The energy of the scattered electrons in these runs will be $\sim$ 5 GeV. Extrapolation of the calibration algorithm to higher energies will be checked using the scintillator hodoscopes.

The two Čerenkov counters in each spectrometer are cylindrical tanks filled with sub-atmospheric CO_2. Their lengths are 2 m and 4 m. The CO_2 gas was chosen as the Čerenkov radiator medium because of its low scintillation and knock-on electron created by the passage of pions. In addition to this, CO_2 is transparent in the ultraviolet region down to 200 nm.

The two scintillator hodoscopes will provide data for a statistical evaluation of possible systematic errors in the lead glass and Čerenkov counter data. They are expected to be instrumental in pion identification for measuring also the asymmetry of inclusive pion yields. The fine segmentation of the hodoscopes was chosen to tolerate the large expected photon and neutron backgrounds and to reconstruct with sufficient resolution the production coordinates of the scattered particles.

The expected angular resolutions in non-bend plane are $\sim \pm 0.3$ mr for both spectrometers. In the bend plane they are $\sim \pm 0.9$ mr for the 4.5° arm and $\sim \pm 0.3$ mr for the 7° arm. The momentum resolution of the system depends on the absolute

value of momentum and varies from $\pm 0.5\%$ to $\pm 1.8\%$ for the 4.5° spectrometer and from $\pm 0.6\%$ to $\pm 3.5\%$ for the 7.0° spectrometer as can be seen in Fig. 11. The Figure also shows the projected energy resolution of the reconfigured ASP shower counter as well as the required momentum resolution that corresponds to the desired x resolution.

The electron trigger will be the logic OR of a combination of the detector signals in coincidence, like C1·C2·SH_L, C1·SH_H, C2·SH_H. C1 and C2 denote the discriminator signals of the two Čerenkov counters. SH_L and SH_H are the shower counter signals for a 'low' and a 'high' discriminator threshold. In addition to the electron trigger there will be a prescaled pion trigger formed by the coincidence of the two hodoscope signals vetoed by the coincidence of the two Čerenkov counters.

APPENDIX

Expressions for k and K (and the corresponding transverse asymmetry factors k' and K') are given below:

$$K = \frac{E\cos\theta}{2x\sigma_{Mott}}\left(\frac{E'\cos\theta}{E + E'\cos\theta}\right), \qquad k = \frac{2xM}{E + E'\cos\theta},$$

$$K' = \frac{E\cos\theta}{2x\sigma_{Mott}} \cdot \frac{1}{\tan\theta}, \qquad k' = \frac{2xM}{E'(1 - \cos\theta)},$$

in terms of the beam energy E, final electron energy E', scattering angle θ, nucleon mass M and the Mott cross section

$$\sigma_{Mott} = \left(\frac{\alpha\cos(\theta/2)}{2E\sin^2(\theta/2)}\right)^2.$$

α is the fine structure constant.

The virtual photon depolarization factor is

$$D = \frac{y(2-y)}{y^2 + 2(1-y)(1+R)},$$

where $y = E - E'/E$ and R is the ratio σ_L/σ_T.

REFERENCES

1. SLAC Proposal E142, E. W. Hughes *et al.* (1989).
2. C. E. Carlson and Wu-Ki Tung,, *Phys. Rev.* **D5**(1972), 721
3. A. J. G. Hey and J. E. Mandula,, *Phys. Rev.* **D5**(1972), 2610
4. E. Leader and M. Anselmino, *Z. Phys.* **C41**(1988), 239
5. Oscar A. Rondon-Aramayo, *The Spin Structure of the Nucleon in a Modified Callaway-Ellis Model*, UVA-INPP-PUB-91-15, Institute of Nuclear and Particle Physics, University of Virginia, Charlottesville, September 1991
6. M. J. Alguard *et al.*, *Phys. Rev. Lett.* **37**(1976), 1261,
   Phys. Rev. Lett. **41**(1978), 70
7. G. Baum *et al.*, *Phys. Rev. Lett.* **51**(1983), 1135
8. The EMC collaboration, J. Ashman *et al.*, *Nucl. Phys.* **B328**(1989), 1
9. J. Ellis and R. L. Jaffe, *Phys. Rev.* **D9**(1974), 1444, **D10**(1974), 1669
10. J. D. Bjorken, *Phys. Rev.* **148**(1966), 1467, *Phys. Rev.* **D1**(1970), 1376
11. H. Burkhardt and W. N. Cottingham, *Ann. Phys. (N.Y.)* **56**(1970), 453
12. W. Wandzura and F. Wilczek, *Phys. Lett.* **B172**(1977), 195
13. R. P. Feynman, *Photon-Hadron Interactions* (Benjamin, New York, 1972)
14. R. L. Heimann, *Nucl. Phys.* **B64**(1973), 429
15. V. M. Belyaev and B. L. Ioffe, *Int. J. Mod. Phys.* **A6**(1991), 1533
16. R. L. Jaffe and Xiangdong Ji, *Phys. Rev.* **D43**(1991), 726
17. K. Hidaka, E. Monsay and D. Sivers, *Phys. Rev.* **D19**(1979), 1503
18. E. Richter-Was, *Acta Phys. Pol.* **B16**(1985), 739
19. M. L. Seely *et al.*, *Nucl. Inst. Meth.* **201**(1982), 303
20. D. G. Crabb *et al.*, *Phys. Rev. Lett.* **64**(1990), 2627

21. T. O. Niinikoski and J. M. Rieubland, *Phys. Lett.* **A72**(1979), 141

22. W. W. Ash, Proc. High Energy Physics with Polarized Beams and Targets, Ed. M.L. Marshak (AIP New York 1976) , 485

23. U. Haertel *et al.*, High Energy Physics with Polarized Beams and Polarized Targets, eds., C. Joseph and J. Soffer, Birkhauser Verlag, Basel (1981) , 447

24. D. G. Crabb *et al.*, Proc. 4th. Intl. Workshop on Polarized Target Materials and Techniques, Bonn 1984, Ed. W. Meyer, 7

25. W. Meyer *et al.*, *Nucl. Instr. Meth.* **215**(1983), 65

26. D. G. Crabb, Proc. High Energy Spin Physics, Bonn 1990, Eds. W. Meyer, E. Steffens, W. Thiel, Springer Verlag 1991, 289

27. M. L. Seely et al., Proc. Int. Conf. on High Energy Spin Physics, Brookhaven 1982, ed. G. Bunce, AIP Conf. Proc. 95(1982), 526

28. T. Maruyama, E. L. Garwin, R. Prepost, G. H. Zapalac, *et al.*, *Phys. Rev. Lett.* **66**, 2376 (1991).

29. T. Nakanishi *et al.*, *Phys. Lett.* **A158**, 345 (1991), and E. L. Garwin, T. Maruyama, R. Prepost, and G. H. Zapalac, to be published

30. Z-E. Meziani, private communication

31. C. Y. Prescott *et al.*, *Phys. Lett.* **B77**, 347 (1978); M. J. Alguard *et al.*, *Phys. Rev. Lett.* **37**, 1261 (1976)

32. G. G. Petratos *et al.*, SLAC-PUB-5678 (1991), presented at the 1991 IEEE Nuclear Science Symposium, Santa Fe, Nov. 1991

33. D. Kawall and Z-E. Meziani, E142 internal report *E142 Threshold Čerenkov Counters* (1990)

34. P. A. Souder, E142 internal report *Hodoscopes for E142* (1990)

35. G. T. Bartha *et al.*, *Nucl. Instr. Methods* **A275**, 59 (1989)

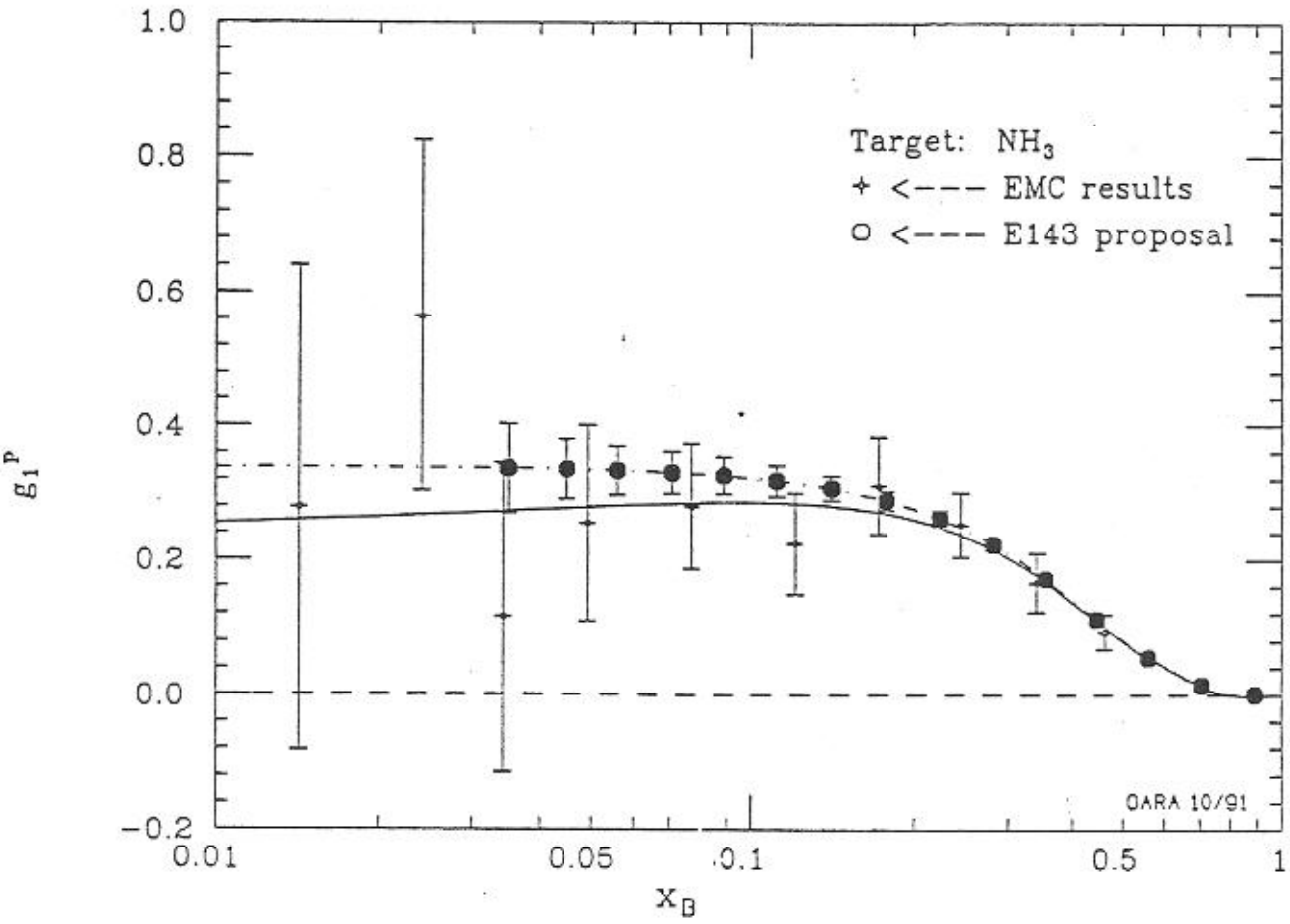

Figure 1.

Fig. 1. – Comparison of the proposed measurements and EMC data. Crosses: EMC data. Full circles: proposed experiment. All errors shown are statistical only. Curves: Solid – EMC fit to $A_1^p \times F_1^p$; Dotdash – g_1^p structure function in a modified Callaway-Ellis model.

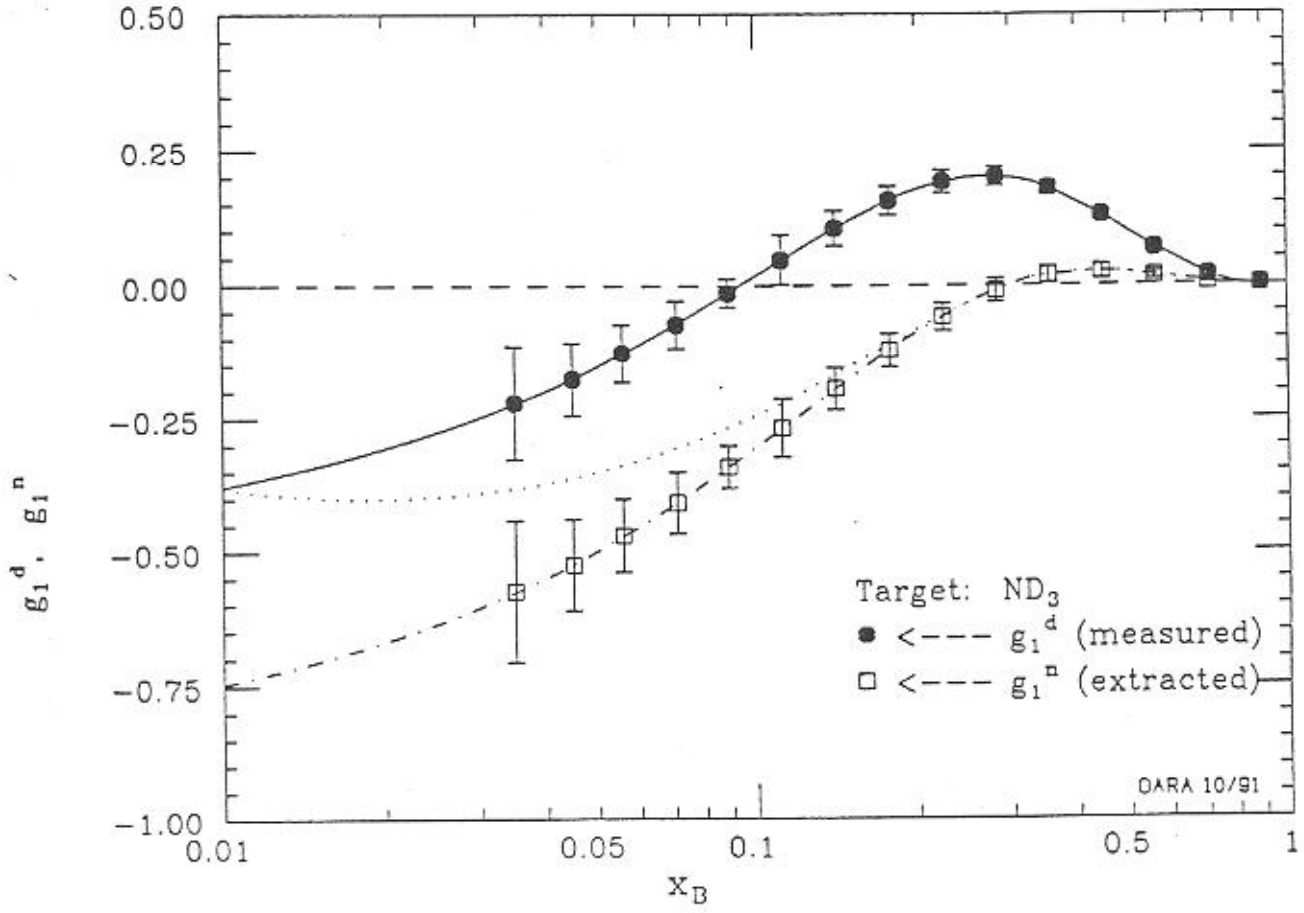

Figure 2.

Fig. 2. – Proposed measurements. Only statistical errors are shown. Full circles: deuterium data. Open squares: extracted neutron results. Curves: Solid – Deuteron g_1^d; Dotdash – Neutron g_1^n structure functions in same Callaway-Ellis model as the proton. Dots – g_1^n extracted from A_1^n and F_2^n.

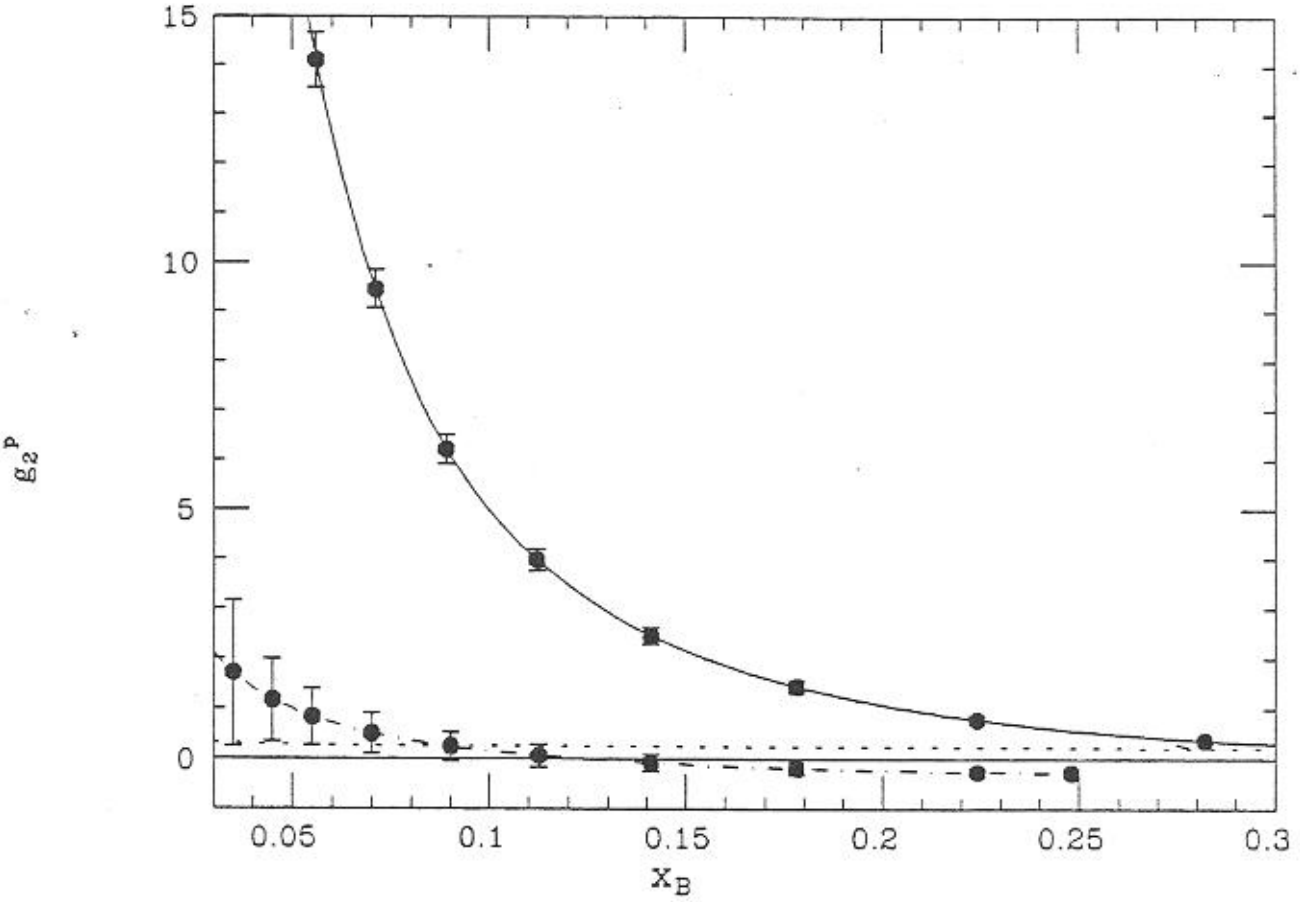

Figure 3.

Fig. 3. – x dependence of the transverse structure function g_2^p . The solid line corresponds to the upper limit from $|A_2| \leq \sqrt{R}$. The dot-dashed line is the twist 2 component of g_2^p from the Wandzura-Wilczek sum rule.[12] The error bars represent the sensitivity of the proposed measurement (statistical uncertainties only). The dotted line is g_1^p , shown for comparison.

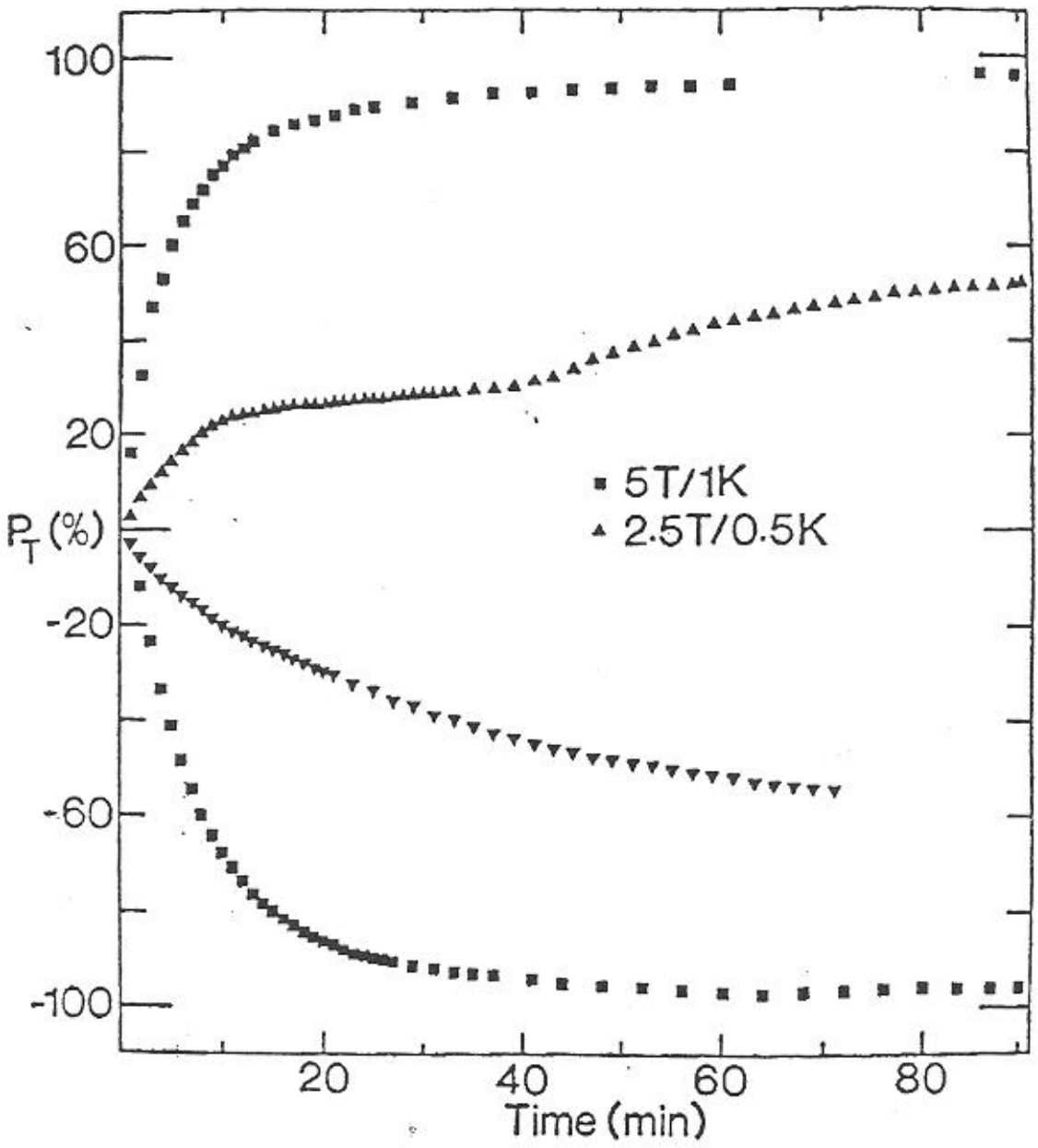

Fig. 4. – The spin polarization of the free protons in NH_3 plotted against the time of microwave irradiation. The new data at 5T and 1K are shown as squares; earlier data at 2.5 T and 0.5 K are shown as triangles.

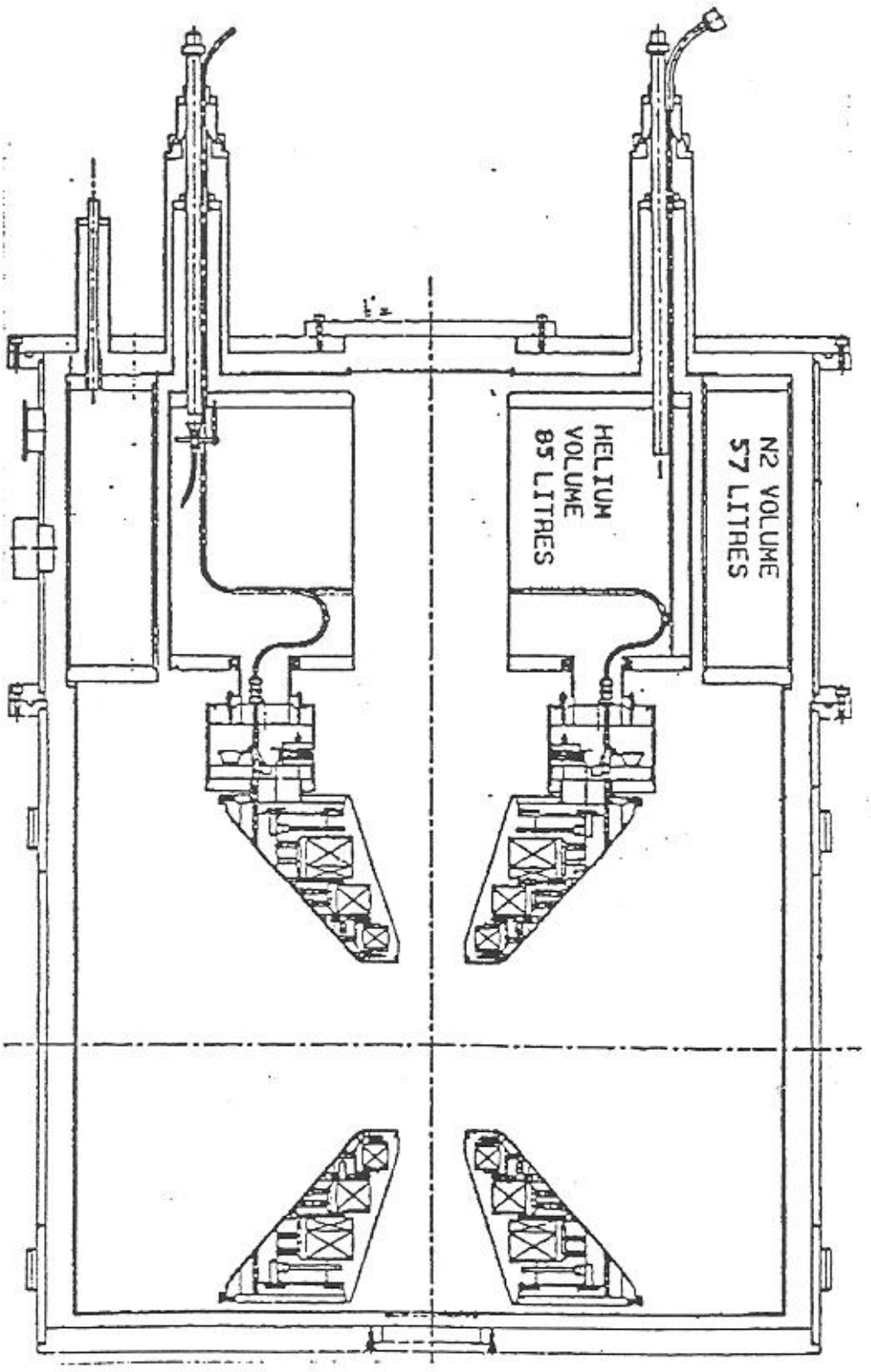

Fig. 5. – A sketch of the croystat and coil for the ammonia target.

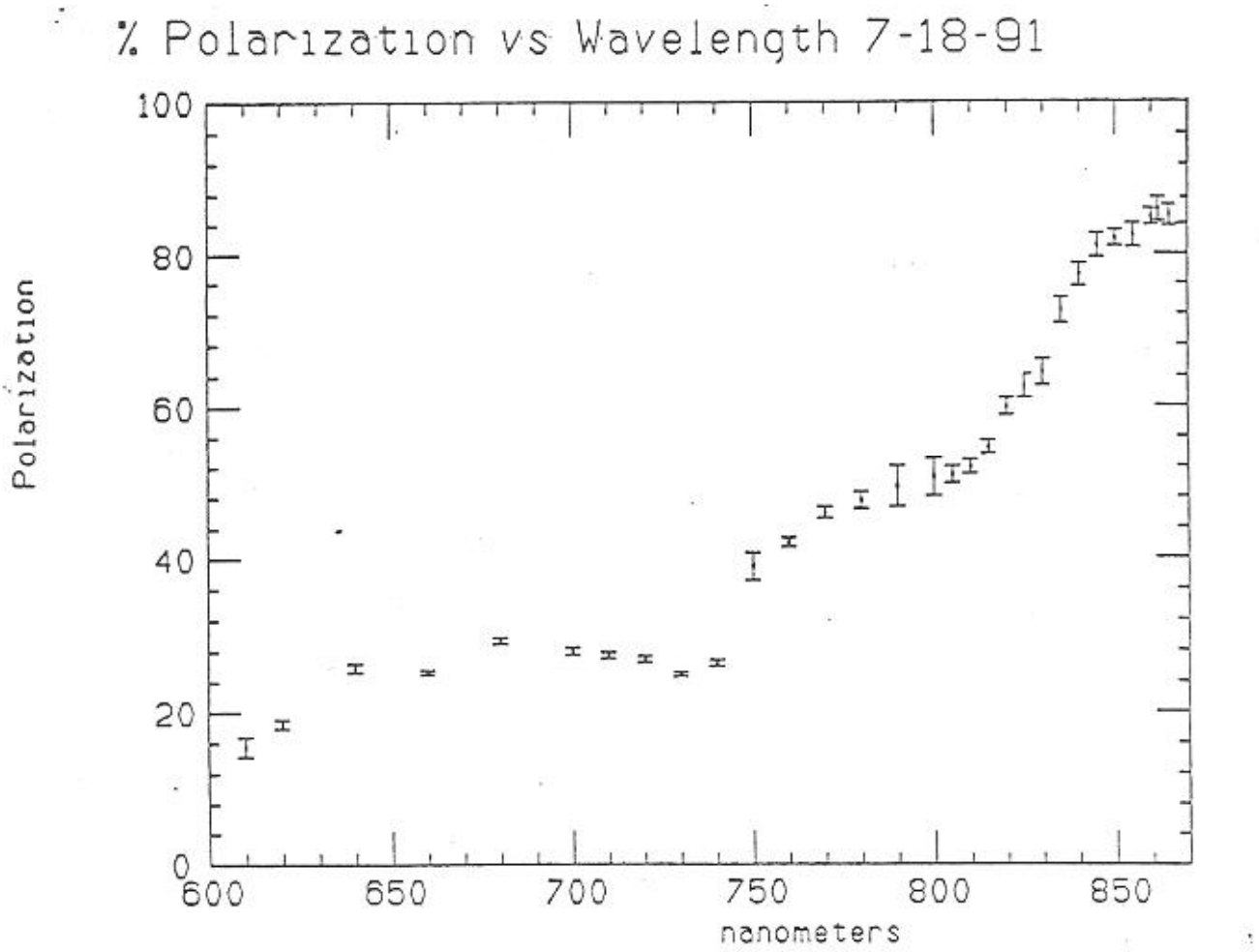

Fig. 6. – Polarization of photoemitted electrons as a function of the incident photon wavelength for a strained gallium-arsenide cathode material.

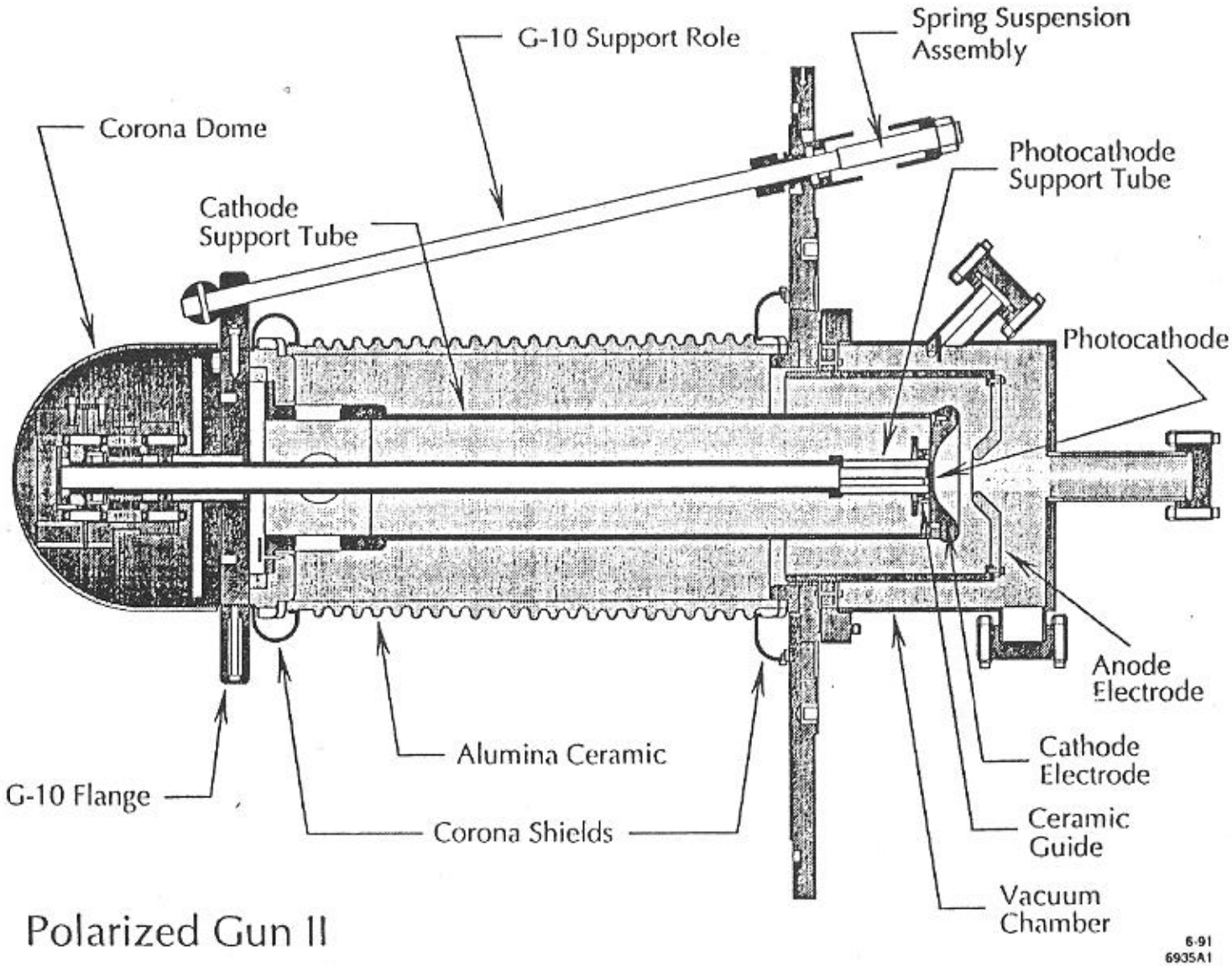

Fig. 7. – The polarized gun structure for the SLAC injector. The gun has been developed for the SLC program, but will also provide polarized beams for the linac long pulse operation for End Station A.

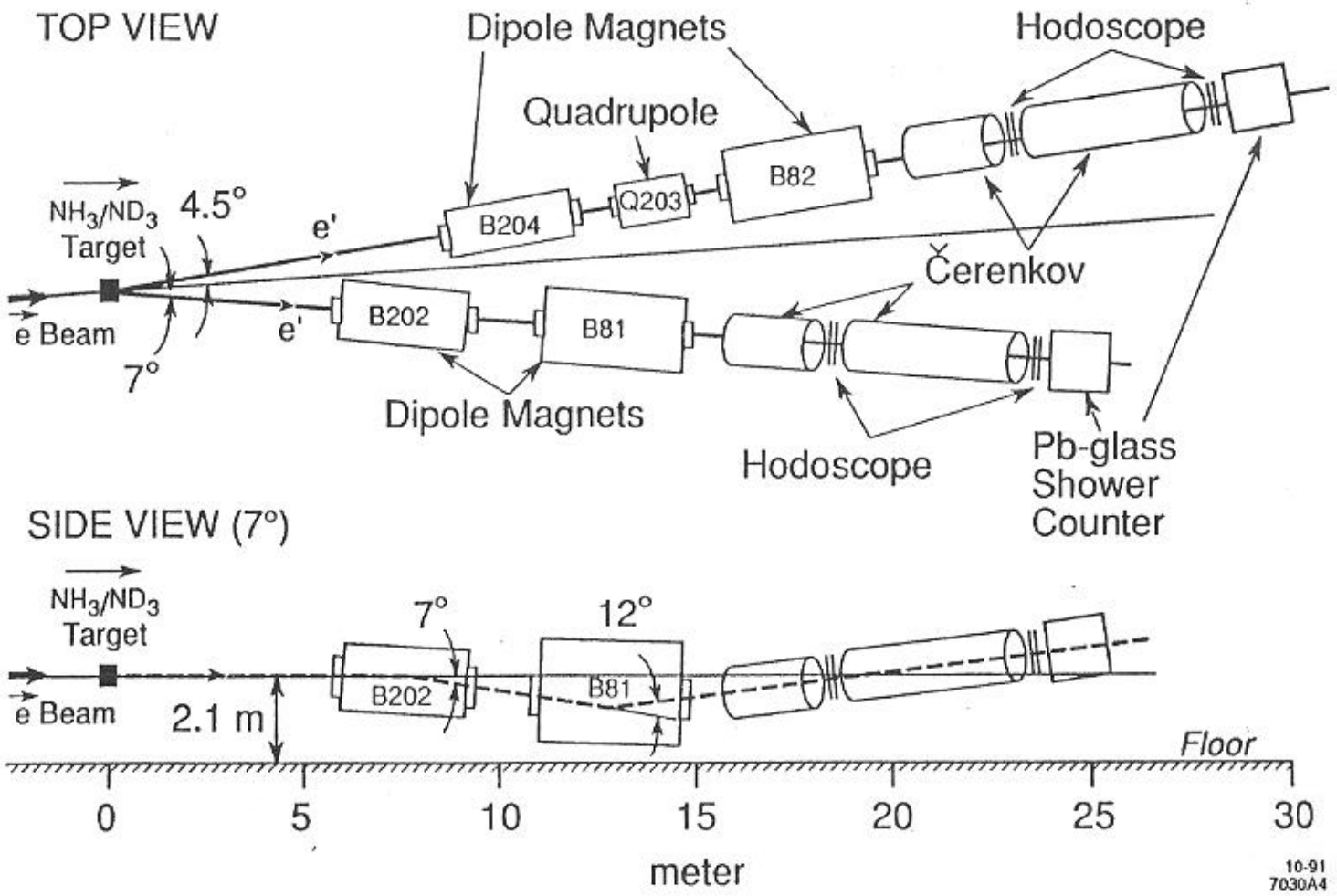

Fig. 8. – The two magnetic spectrometer systems and detector packages to be used in this experiment. The dipoles B202, B204 and the quadrupole Q203 are magnetic elements of the SLAC 20 GeV/c spectrometer. The dipoles B81 and B82 are elements of the SLAC 8 GeV/c spectrometer.

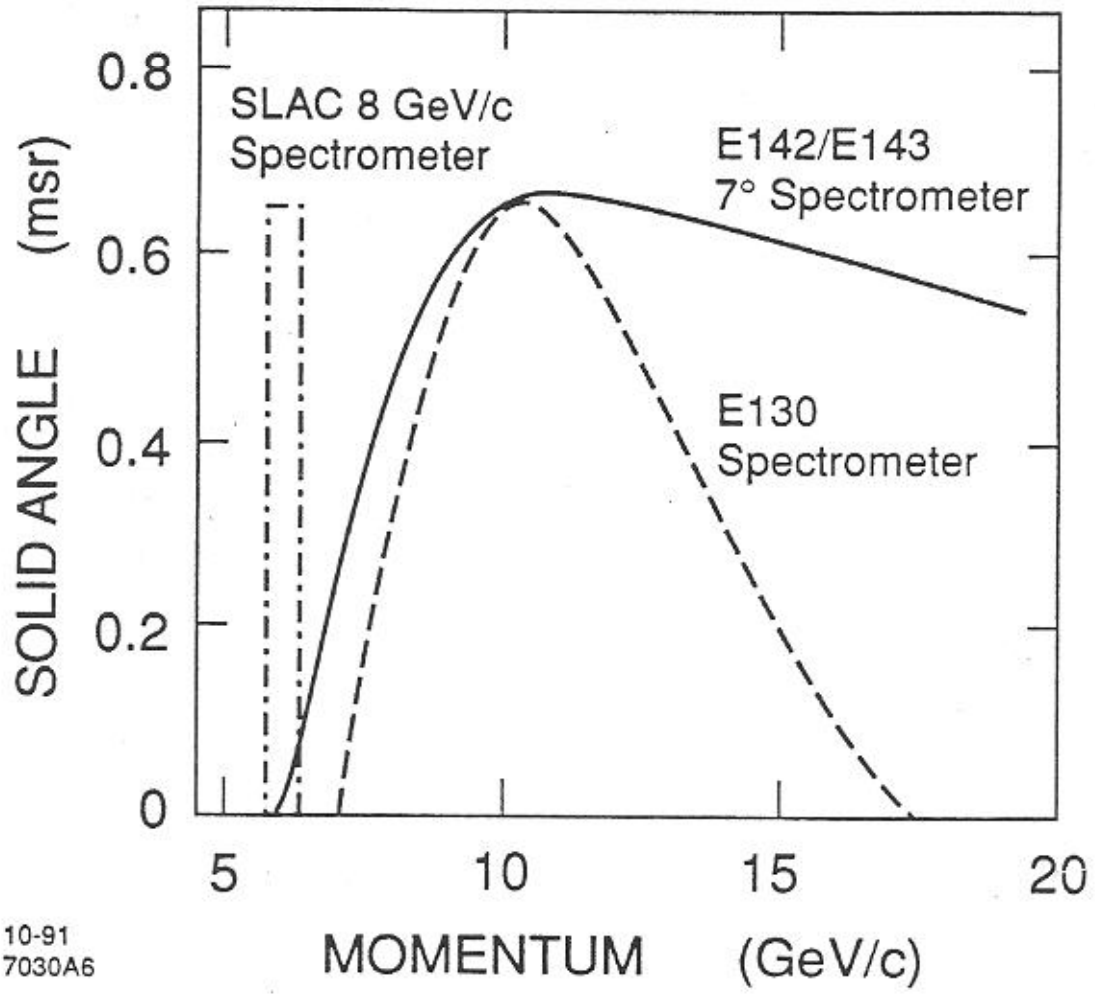

Fig. 9. – The solid angle of the 7.0° magnetic spectrometer system plotted versus momentum. The acceptances of the E130 spectrometer and of the SLAC 8 GeV/c spectrometer are shown for comparison.

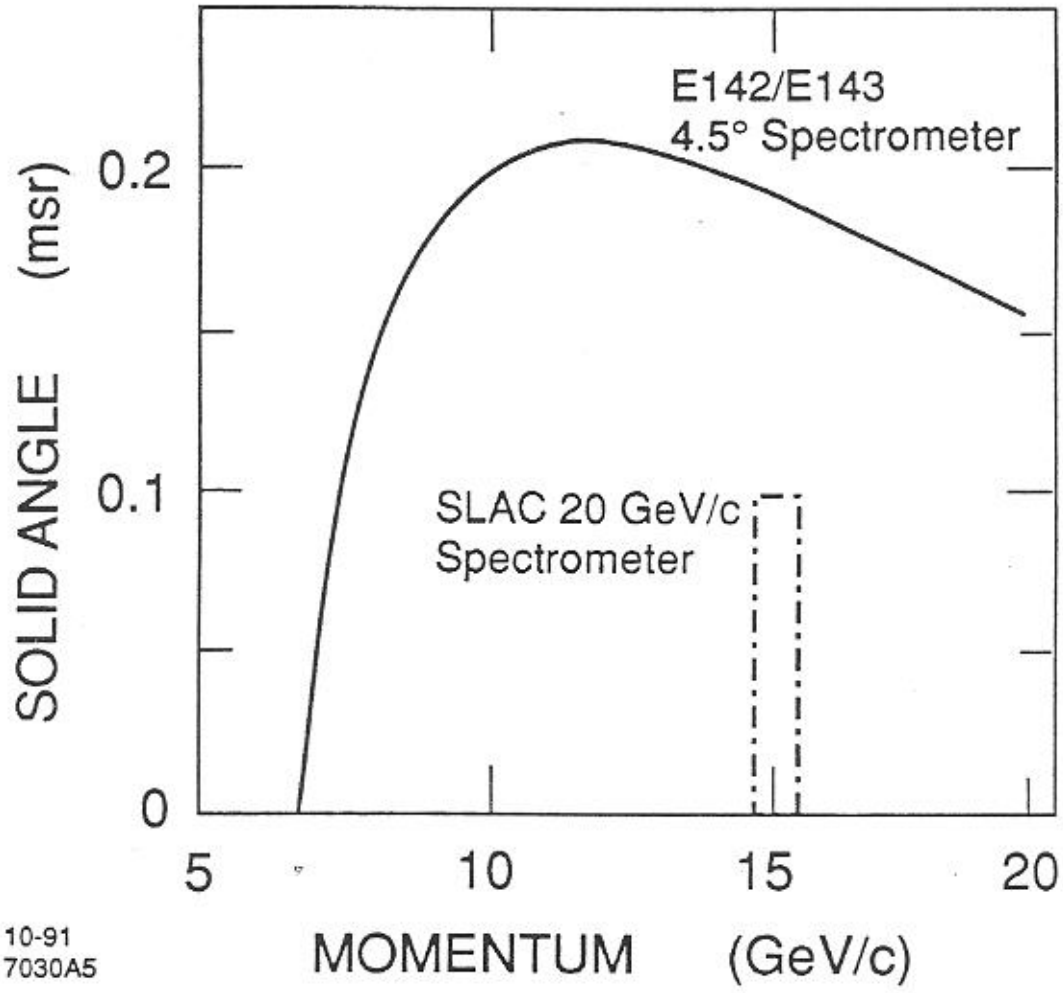

Fig. 10. – The solid angle of the 4.5° magnetic spectrometer system plotted versus momentum. The acceptance of the SLAC 20 GeV/c spectrometer is shown for comparison.

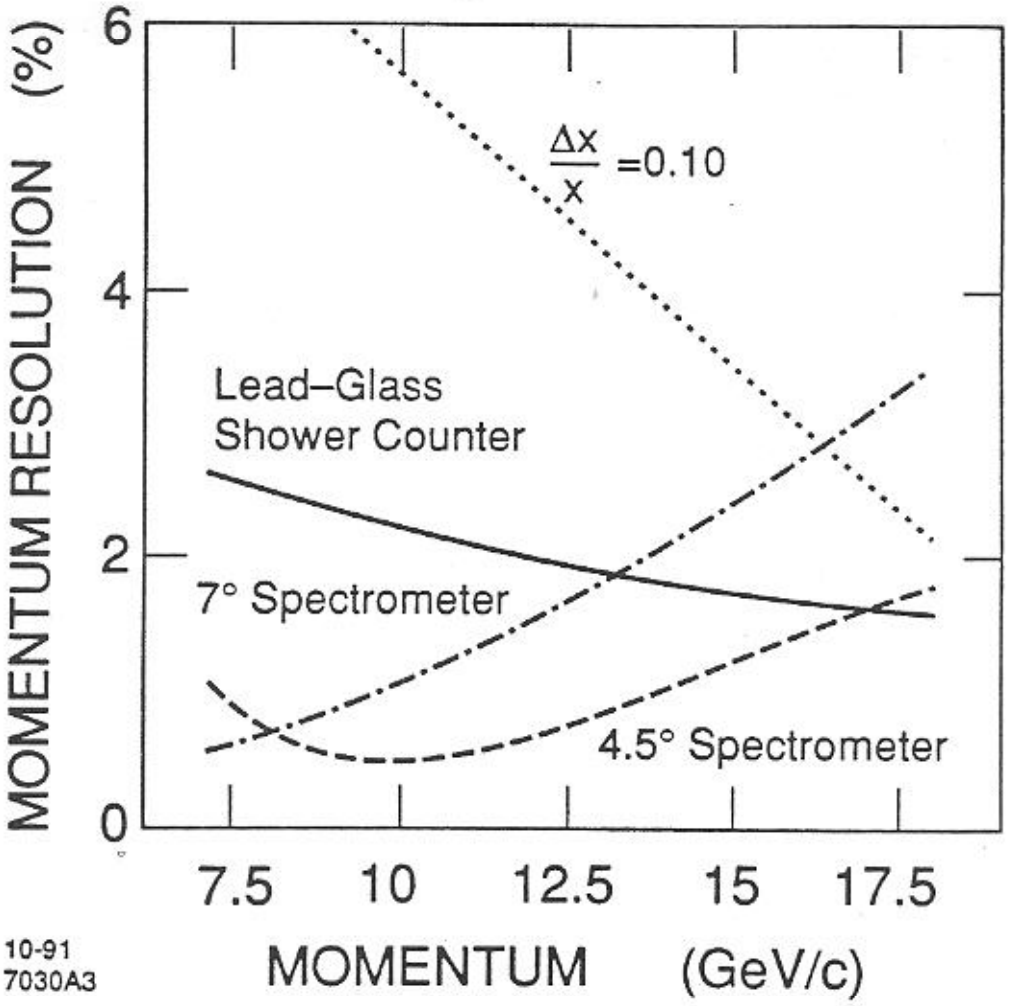

Fig. 11. – Expected momentum resolution of the two magnetic spectrometer systems. Also shown is the expected energy resolution of the reconfigured ASP lead glass shower counter as well as the required momentum resolution that corresponds to the desired x resolution.